GROWTH AND COLLAPSE OF NANOVOIDS IN TANTALUM MONOCRYSTALS LOADED AT HIGH STRAIN RATE

Y. Tang[1], E. M. Bringa[2], B. A. Remington[3], and M. A. Meyers[1]

[1]*University of California, San Diego, La Jolla, CA, 92093*
[2]*CONICET & Instituto de Ciencias Básicas, Univ. Nac.Cuyo, Mendoza, 5500 Argentina*
[3]*Lawrence Livermore National Laboratory, Livermore, CA, 94550*

Abstract. Shock-induced spall in ductile metals is known to occur by the sequence of nucleation, growth and coalescence of voids, even in high purity monocrystals. However, the atomistic mechanisms involved are still not completely understood. The growth and collapse of nanoscale voids in tantalum are investigated under different stress states and strain rates by molecular dynamics (MD) simulations. Three principal mechanisms of deformation are identified and quantitatively evaluated: shear loop emission, prismatic loop formation, and twinning. Dislocation shear loops expand as expected from a crystallographic analysis, and their extremities remain attached to the void surface in tension (if there is no dislocation reaction or cross slip), but can detach in compression and form prismatic loops due to cross slip and reactions. Prismatic loops that detach from the void are also formed by reaction of multiple shear loops sharing the same <111> slip direction during hydrostatic loading. Nanotwins form preferably upon both uniaxial and hydrostatic tensile stress. The void-size effect on plasticity is studied via MD simulations and is modeled based on the shear loop emission mechanism. The stresses required for generation of a free surface step, dislocation and bow are calculated by continuum dislocation theory. The predictions agree well with MD simulation results.

Keywords: Void growth, dislocation loop, ductile failure, molecular dynamics.
PACS: 60.20.F-, 61.72.Qq, 61.72.Lk.

INTRODUCTION

The nucleation, growth and coalescence of voids lead to ductile fracture and spalling (induced by reflected tensile pulses) of metals. Although this phenomenon was realized as early as 1949 by Tipper [1], and a complete account was given by Dodd and Bai [2], the atomistic mechanisms are still not completely understood. An analytical model based on shear and prismatic loops emission was proposed by Lubarda, et al. [3] in 2004, followed by a considerable effort in MD simulations of void growth, which confirmed the emission of shear loop in FCC metals [4]. For BCC metals, prismatic dislocation loops and twinning were observed by Rudd [5]. The goal of the current investigation is to extend the study by Bringa, et al. [4] to a BCC metal and to develop a mechanistic understanding of the deformation mechanisms and void-size effect.

COMPUTATIONAL METHODS

MD simulations were carried out using LAMMPS [6] with the Extended Finnis-Sinclair (EFS) potential [7]. The monocrystal tantalum domain was a cube with a spherical void at the center. The void radius R varied from 0 ~ 30 nm. Simulation box size was L = 30, 50, 60, 80, 100, 200 and 400 a_0, where a_0 = 0.303 nm is the lattice constant, with total number of atoms being N_{sample}

Shock Compression of Condensed Matter - 2011
AIP Conf. Proc. 1426, 1255-1258 (2012); doi: 10.1063/1.3686508

= 0.054, 0.25, 0.432, 1.024, 2, 16 and 128 millions. Periodic boundaries were applied in all directions. The stress state included uniaxial tensile and compressive strain along [100], and triaxial (hydrostatic) tensile and compressive strain along [100], [010] and [001]. All simulations were done at an initial temperature of 300 K and without any temperature control during loading, to capture temperature effects related to plasticity. The strain rate varied from 10^8 s^{-1} to 10^9 s^{-1}. Visualization of defects was conducted in VMD [8] with a filter using common neighbor analysis (CNA) [9].

The generalized stacking fault energies for the primary slip systems, {110}/<111> and {112}/<111> were calculated using molecular statics. For each slip system, periodic boundaries were applied in the two directions parallel to the slip plane of a 24 nm cubic crystal, and the crystal was free to move along the two directions perpendicular to the slip direction. Only relaxations along the slip direction of the generalized fault were not allowed.

RESULTS AND DISCUSSION

The generalized stacking fault energies $\gamma(\mathbf{f})$ for {110} and {112} slip planes gliding along <111> directions are shown in Fig. 1, where **f** is the displacement vector, f is the magnitude of **f** and the magnitude of the Burgers vector **b** is b = |1/2<111>|. Comparisons with ab initio calculations [10], the model generalized pseudopotential theory (MGPT) [11], first-principles-based force fields method (qEAM) [12] and angular-dependent potential (ADP) [10] are also included in Fig. 1. Reasonable agreement is found, especially with MGPT and ADP, validating the use of this extended Finnis-Sinclair potential for plasticity studies.

No minimum energy points are found for the two slip systems studied here, which means stacking faults are unstable. The $\gamma(f) \sim f$ curve for {110} planes has the lowest energy ({110} planes are the closest-packed planes for BCC) and is symmetric with respect to $f = b/2$, which means gliding along [111] and its opposite direction are equivalent. On the other hand, the curve for {112} planes has higher energy and is asymmetric; thus, gliding in one [111] direction (twinning direction) is easier than in its opposite direction (anti-twinning direction).

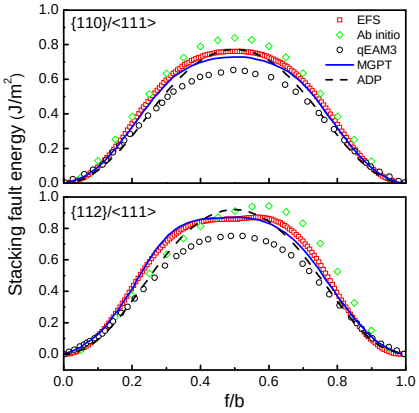

Figure 1. Generalized stacking fault energies γ (f) for {110}/ <111> and {112}/<111> slip systems using EFS potential and comparison with other calculations [10-12].

For a 3.3 nm radius void, different stress states and strain rates are applied and three principal deformation mechanisms are identified: (a) shear loop emission and expansion; (b) prismatic loop formation by reaction of multiple shear loops sharing the same <111> slip direction, or by the cross slip and reaction of screw components of a single shear loop; and (c) twinning.

Typical snapshots of defect evolution for R = 3.3 nm are shown in Figs. 2-5. In Fig. 2, planar shear loops nucleate from the void surface and expand in {112} slip planes. Only four {112} slip systems with higher Schmid factor (see detailed discussion in Ref. 13) can be activated under uniaxial strain loading, and the extremities of the shear loops remain attached to the void surface in the absence of dislocation reaction and cross slip.

For hydrostatic loading, all twelve {112} slip systems can be activated due to the equal resolved shear stress under this loading condition. There are three different activated {112}/<111> slip systems sharing the same <111> direction, as shown in Fig. 3. As these three shear loops expand, their screw components meet and react, canceling each other (the screw components have the same Burgers vector but opposite dislocation line directions). Only edge components are left and they connect with each other to form a prismatic dislocation loop (triangular shaped, as seen in Fig. 3).

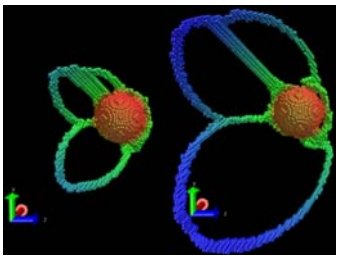

Figure 2. Snapshots of defect evolution showing emission and expansion of shear loops (uniaxial tensile strain, 10^8 s^{-1}). Only non-BCC atoms are shown.

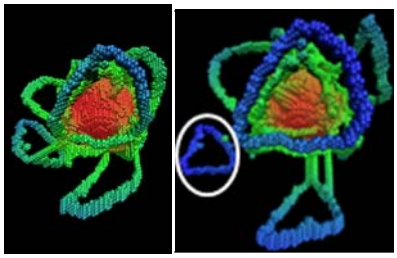

Figure 3. Formation of prismatic loops (marked by white circle) by reaction of multiple shear loops sharing the same <111> direction (hydrostatic tension, 10^8 s^{-1}).

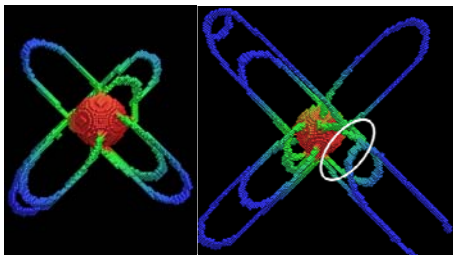

Figure 4. Prismatic loop formation by cross slip and reaction of a single shear loop (uniaxial compressive strain, 10^8 s^{-1}).

Besides dislocation reaction, prismatic loops can also be formed by cross slip induced reaction. As shown in Fig. 4, the two screw components of a single non-planar shear loop cross slip in three different {110} planes sharing the same <111> slip direction, and cancel each other when they meet, forming a prismatic loop that detaches from the void surface (marked in white circle in Fig. 4).

When the strain rate is increased, twins form (in tension) instead, as shown in Fig. 5. The stress states and strain rates studied for R = 3.3 nm void and their corresponding operating deformation mechanisms under these conditions are summarizes Table 1.

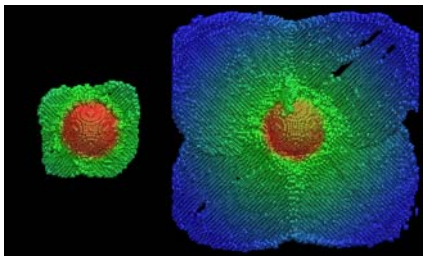

Figure 5. Formation of twins (uniaxial tensile strain, $10^9 s^{-1}$).

For different void sizes, R = 0 ~ 30 nm, MD simulations were carried out under uniaxial tensile strain at strain rates of both $10^8 s^{-1}$ and $10^9 s^{-1}$. The normalized von Mises stresses at which plasticity occurs for different void size R are plotted in Fig. 6 ($G_{<111>}$ = 52.8 GPa, $\upsilon_{<111>}$ = 0.223 and b = 0.286 nm). As seen in Fig. 6, for smaller radii ($R/b \leq 1 \sim 2$), the stresses asymptotically approach a value of $\sigma_{vM}/ G_{<111>} \approx 0.14$, which is the required stress for homogeneous nucleation (HN) of defects in perfect sample (R = 0). As the void size increases, the nucleation stress decreases, and approaches a constant value of 0.055 when the void size R/b exceeds ~ 100.

The initiation of plasticity, namely emission of shear dislocation loops, is modeled based on dislocation theory. The nucleation stress required for producing a shear dislocation loop includes creation of a new surface step [14] τ_1 and generating and bowing a dislocation loop to a

TABLE 1. Summary of three deformation mechanisms (R=3.3 nm): emission of shear loops (S), formation of prismatic loops (P) and twinning (T).

	Void growth		Void collapse	
Strain rate	hydrostatic tension	uniaxial tensile strain	hydrostatic compression	uniaxial compressive strain
10^8 s^{-1}	**S+P**	**S** (axially symmetric stress field)	**S+P** (cross slip of 1/2<111> screw dislocations)	**S+P** (cross slip of 1/2<111> screw dislocations)
10^9 s^{-1}	**T** (generated by 1/2<111> screw dislocation)	**T** (generated by 1/2<111> screw dislocation)		

radius R_1that is a fraction of the void radius R, τ_2,

$$\tau_1 = \frac{2\gamma}{\pi\rho b}, \quad \tau_2 = \frac{Gb(2-\nu)}{4\pi(1-\nu)R_1}\ln\frac{2R_1}{\rho b} \qquad (1)$$

where γ is surface energy (2.49 J/m^2), ρb is the radius of the dislocation core, G is shear modulus, and υ is Poisson's ratio. The local maximum shear stress $\tau_{max}=\tau_1+\tau_2$ near the void due to stress concentration is converted to the global von Mises stress by solving the elastic stress field around the void, $\sigma_{vM} = 0.448\tau_{max}$. This analytical model matches the computational predictions in Fig. 6 very well for $\rho = 1$ and $R_1 = R/2$, and is not expected to be valid when the loop radius is smaller than the dislocation core (R/b smaller than 1~2).

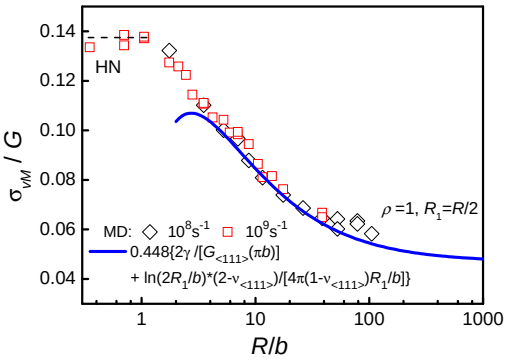

Figure 6. Normalized von Mises stress for defect nucleation as a function of normalized void radius R/b.

CONCLUSIONS

Void growth and collapse in BCC tantalum monocrystals are studied using MD simulations. Three principal deformation mechanisms are identified: shear loop emission, prismatic loop formation (by dislocation reaction, cross slip and reaction) and twinning. The effects of stress state (uniaxial vs. hydrostatic; tension vs. compression) and strain rate on the deformation mechanisms are discussed. The nucleation stress for plasticity is found to be void-size dependent: the increase in void size reduces the required stress for nucleation of defects. An analytical dislocation-based model is proposed to account for the void-size dependence of plasticity, and is found to agree well with the MD simulation results.

ACKNOWLEDGEMENTS

Funding was provided by the University of California Research Laboratory Program. E.M.B. thanks computer time at the SUMO cluster at the Centro Atomico Bariloche, at the TWISTER cluster at the Instituto Tecnologico Universitario in Mendoza.

REFERENCES

1. Tipper, C. F., "The fracture of metals," Metallurgia **39**, pp 133-137 (1949).
2. Dodd, B., Bai, Y., Ductile Fracture and Ductility, pp. 97 (Academic Press, London, 1987).
3. Lubarda, V. A., et al., "Void growth by dislocation emission," Acta Mater. **53**, pp 1397-1408 (2004).
4. Bringa, E. M., et al., "Void initiation in fcc metals: Effect of loading orientation and nonacrystalline effects," Acta Mater. **58**, pp 4458-4477 (2010).
5. Rudd, R. E., "Void growth in bcc metals simulated with molecular dynamics using the Finnis-Sinclair potentials," Phil. Mag. **89**, pp 3133-3161 (2009).
6. Plimpton, S. J., "Fast parallel algorithms for short-range molecular-dynamics," J. Comp. Phys. **117**, pp 1-19 (1995).
7. Dai, X. D., et al., "Extended Finns-Sinclair potentials for bcc and fcc metals and alloys," J. Phys: Condens. Matter **18**, pp 4527-4542 (2006).
8. Humphrey, W., et al., "VMD: Visual molecular dynamics," J. Molec Graphics **14**, pp 33-38 (1996).
9. Tsuzuki, H., et al., "Structure characterization of deformed crystals by analysis of common atomic neighborhood," Comput. Phys. Comm. **177**, pp 518-523 (2007).
10. Mishin, Y., Lozovoi, A. Y., "Angular-dependent interatomic potential for tantalum," Acta Mater. **54**, pp 5013-5026 (2006).
11. Yang, L. H., et al., "Accurate atomistic simulation of (a/2) < 111 > screw dislocations and other defects in bcc tantalum," Phil. Mag. **81**, pp 1355-1385 (2001).
12. Wang, G. F., et al., "Atomistic simulations of kinks in 1/2a < 111 > screw dislocations in bcc tantalum," Phys Rev B **68**, 224101 (2003).
13. Tang, Y., et al., "Growth and collapse of nanovoids in tantalum monocrystals," Acta Mater. **59**, pp. 1354-1372 (2011).
14. Weertman, J., Dislocation Based Fracture Mechanics 194-195 (World Scientific, Singapore, 1996).